Related Articles

Chiral tunneling in trilayer graphene
Appl. Phys. Lett. 100, 163102 (2012)

Analytical models of approximations for wave functions and energy dispersion in zigzag graphene nanoribbons
J. Appl. Phys. 111, 074318 (2012)

Effect of in-situ oxygen on the electronic properties of graphene grown by carbon molecular beam epitaxy grown
Appl. Phys. Lett. 100, 133107 (2012)

Oxygen density dependent band gap of reduced graphene oxide
J. Appl. Phys. 111, 054317 (2012)

Electronic structures of graphane with vacancies and graphene adsorbed with fluorine atoms
AIP Advances 2, 012173 (2012)

Additional information on J. Appl. Phys.

Journal Homepage: http://jap.aip.org/

Journal Information: http://jap.aip.org/about/about_the_journal

Top downloads: http://jap.aip.org/features/most_downloaded

Information for Authors: http://jap.aip.org/authors

Electronic states in heterostructures with piece-wise uniform Dirac cones

Hai-Yao Deng[a)]

Department of Applied Physics, The Hong Kong Polytechnic University, Hung Hom, Hong Kong

We discuss graphene physics that are associated with Fermi velocity rather than bandgap or external potential. Such physics are illustrated with a simple junction that is comprised of two uniform electrodes bridged by a central uniform channel. The main difference between these components is supposed to come at their Fermi velocities (Dirac cone slopes), which take different values: ν_0 in the electrodes and v in the channel. This junction can be fabricated, for example, by depositing a single-layer graphene on prepatterned substrate. Both scattering states and localized states have been explored. Making full analog with optics, the discussions have been focused on these aspects: refraction, total internal reflection (TIR), and transmission. Regarding them, Snell's law and the TIR critical angle have been derived and the TIR impacts on transmission have been calculated. Potential applications of this junction have been discussed. In particular, we found that, an electrical switch and an electron box can be made of it. © *2012 American Institute of Physics*.
[doi:10.1063/1.3681900]

I. INTRODUCTION

Since its isolation in 2004 by Geim *et al.*,[1] graphene has engrossed immense interests for its properties promising in applications[2] and fundamental physics.[3] Pristine single-layer graphene (SLG) consists of two distinct types of carbon sublattices, A and B, arranged on a honeycomb lattice. The resulting band structure features two valleys or say Dirac cones, K and K' in the Brillioun zone. In the vicinity of each valley, the electronic dispersion relation is linear and characterized by the Fermi velocity, v_F, thus rendering neutrino-like physics described by the massless Dirac equation.[4] Relativistic quantum phenomena could then be explored on a bench-top lab. Interesting physics such as relativistic quantum Hall effect[5] and Klein tunneling[6] have been confirmed in this material.

Being a low dimensional system, SLG has been shown prone to many-body effects such as line broadening[7,8] and exciton formation.[9–11] In particular, v_F can be renormalized.[12] *Ab initio* calculations[13] have confirmed the linear dispersion around the Dirac cones but giving an estimate of v_F about $15\%-20\%$ lower than experimental value. The enhancement of v_F due to electron−electron and electron−phonon interactions has been extensively studied[8,14] and it is concluded that, to produce the observed value, both types of interactions must be taken into account.[15] Work along this line has also revealed the great relevance of substrate screening in determining v_F, which therefore offers a simple route to tune v_F. Heterostructures and superlattice consisting of piece-wise uniform v_F can then be created, for example, by precipitating SLG on prepatterned substrate. Artificial architectures have been the hub to novel phenomena such as electron supercollimation[16] and new generation of massless Dirac fermions.[17]

Recently much attention has been invested in bi-layer graphene (BLG), whose properties were demonstrated depending on the fault angle ϑ.[18–20] In the most often seen BLG, such as the Bernal and AA-stacking ones, ϑ are multiples of $\pi/3$, although BLG with $\vartheta \neq$ multiples of $\pi/3$ have also been obtained e.g., through epitaxial growth on SiC substrates.[21] Surprisingly, in a considerably wide range of ϑ, the band structure (around the valleys) of BLG were found nearly identical to that of SLG, except for the difference in v_F,[18,20] which can be tuned by varying ϑ, thus offering another route to build the aforementioned artificial structures.

In the present paper, we investigate one of the simplest versions of such structures: a junction as portrayed in Fig. 1, where a channel is connected to two electrodes. The electrodes are taken of the same properties, while the channel constitutes the scattering area. We are basically interested in the scattering states, but attention will also be paid to possible localized states. Two-component Dirac equations will be employed, which should be realistic as long as the long wavelength phenomena are concerned. Inter-valley transitions are ignored so that it suffices to focus on a single valley. The Hamiltonian is written as

$$H = v_F(x)\vec{\sigma} \cdot \vec{p} + m(x)\sigma_z, \qquad (1)$$

where $v_F(x) = v + (v_0 - v)[\Theta(-x) + \Theta(x - L)]$ and $m(x) = m[\Theta(x) + \Theta(L - x)]/2$, Θ being the step function. In this choice, v and v_0 stand for the Fermi velocities in the channel and the electrodes, respectively. The mass m is included for a more complete study. One should be cautioned that, the pseudospin denoted by the Pauli matrices $\vec{\sigma} = (\sigma_x, \sigma_y)$ (and σ_z) can bear quite different physical contents under different occasions. So, it is essential to ensure the same physical content throughout the device. For SLG device, $\vec{\sigma}$ always refers to the A- and B-sublattice and the condition is satisfied automatically. However, for BLG device, what $\vec{\sigma}$ refers to hinges on ϑ. Thus, the pseudospin in general refers to different
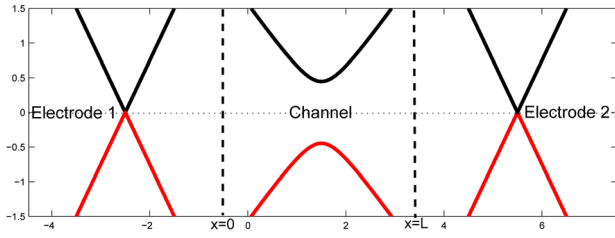
a)Electronic mail: dengstonehiyok@gmail.com.

FIG. 1. (Color online) A sketch of the graphene device: two electrodes connected to the channel along the x-direction. The system is infinite in the y-direction. In the electrodes, $m = 0$ and $v_F = v_0$. In the channel of width L, $v_F = v = \eta v_0$ and m may not be zero.

states in the electrodes than in the channel. Nonetheless, if ϑ takes close values in these regions, the physical contents of $\vec{\sigma}$, though differing, are expected to be comparable. In this case, one may approximately use the same $\vec{\sigma}$ across the entire device.

II. SCATTERING STATES AND ELECTRONIC TRANSMISSION

The regional wave functions can be obtained piecewisely and the global wave function Ψ results by sewing them together under proper boundary conditions. These conditions can be derived from the Schrödinger equation $(E - H)\Psi = 0$ (E being the energy with Ψ) and we obtain $lim_{\epsilon \to 0} \int_{x'-\epsilon}^{x'+\epsilon} H\Psi dx = 0$ for any x', which can be satisfied if the two-component spinor Ψ is continuous everywhere.

We at first consider scattering states with positive energy (while negative energy ones can be obtained via particle-hole transformation). Let's assume the device extends enough in the y-direction so that the boundary effects along this direction may be neglected. Thus, we may write $\Psi(x, y) = f_{k_y}(y)\Phi(x)$, where k_y (which is always real) represents the y-component of the momentum and $-\hbar^2 \partial_y^2 f_{k_y}(y) = \hbar^2 k_y^2 f_{k_y}(y)$. The Φ with appropriate asymptotic behaviors at $|x| \sim \infty$ can then be formed as

$$\Phi_L = e^{ik_0 x}\begin{pmatrix} e^{-i\theta} \\ 1 \end{pmatrix} + r e^{-ik_0 x}\begin{pmatrix} -e^{i\theta} \\ 1 \end{pmatrix}$$
$$\Phi_R = t e^{ik_0 x}\begin{pmatrix} e^{-i\theta} \\ 1 \end{pmatrix} \quad (2)$$
$$\Phi_C = A e^{ikx}\begin{pmatrix} \phi \\ 1 \end{pmatrix} + B e^{-ikx}\begin{pmatrix} -\phi' \\ 1 \end{pmatrix}$$

where $\Phi_{L,R,C}$ are the regional wave functions corresponding to the left electrode, the right electrode and the channel, respectively, and we have set $k_0 + ik_y = \sqrt{k_0^2 + k_y^2}e^{i\theta}$, k_0 being real all the time. In addition, r and t stand for respectively the reflection and transmission coefficients, implying $|r|^2 + |t|^2 = 1$ always. Besides, k and k_0 represent the x-component of the momentum in the channel and the electrodes, respectively. The energy carried by the incident electron is therefore written as $E = \pm\hbar v_0 \sqrt{k_0^2 + k_y^2}$. Due to particle-hole symmetry, we only need consider when $E \geq 0$.

For $(E^2 - m^2)/(\hbar^2 v^2) \geq k_y^2$, there is always a transmitted mode and a reflected mode in the channel. The momen-

tum k is real while φ and φ' are simply phase factors. They are given by

$$k = \sqrt{\frac{E^2 - m^2}{\hbar^2 v^2} - k_y^2}(\phi, \phi') = \frac{\hbar v \sqrt{k^2 + k_y^2}}{E - m}(e^{-i\varphi}, e^{i\varphi}) \quad (3)$$

On the other hand, if $(E^2 - m^2)/(\hbar^2 v^2) < k_y^2$, it will be an evanescent and a growing mode that enter Φ_c, in which case the k becomes pure imaginary and so do ϕ and ϕ'. Writing $k = i\kappa$, one has

$$\kappa = \sqrt{k_y^2 - \frac{E^2 - m^2}{\hbar^2 v^2}}(\phi, \phi') = i\frac{\hbar v}{E - m}(\kappa - k_y, \kappa + k_y). \quad (4)$$

Thus the transmission is expected to depend on the incidence angle θ.

Before moving on, we discuss a resemblance with optics. Since our primary interest is to explore the nonuniform Dirac cone physics, we assume vanishing mass $m = 0$ for the moment. This resemblance consists mainly of the fact that, both a light ray and an electron beam in graphene bear a linear dispersion. When a ray incidents from one medium upon another, refraction can happen according to Snell's law. Indeed, this law also holds exactly for an electron beam. Let's call θ and φ the incidence and refraction angle, respectively. A refractive index can thus be defined as $n = \sin\theta/\sin\varphi$. Since $m = 0$, one has $\sin\theta = (\hbar v_0 k_y)/E$ and $\sin\varphi = (\hbar v k_y)/E$, whence $n = v_0/v \equiv \eta^{-1}$, which is the Snell's law for graphene electrons. Another point concerns total internal reflection (TIR): a light ray can be totally reflected back when incidenting at a small angle from an optically dense medium into a less dense one. Now we show that this also takes place to the electrons. Note that $k_0^2 - k^2 = k_0^2 f(\theta, \eta)$, where $f(\theta, \eta) = (\eta^2 - 1)/(\eta^2 \cos^2\theta)$. When $f(\theta, \eta) > 1$, k becomes imaginary and TIR occurs. The critical angle is

$$\theta_c = \cos^{-1}\sqrt{\frac{\eta^2 - 1}{\eta^2}}. \quad (5)$$

The as-described optic-electronic analogs may help designing new electronic devices based on graphene structures. In what follows, we demonstrate that, the conductance of the device shown in Fig. 1 can be drastically (but not completely due to wave tunneling) suppressed via TIR.

The transmission, $T_\theta(E) = |t|^2$, can be found by applying the boundary conditions to Φ at both $x = 0$ and $x = L$. The calculation of t is straightforward and we jot down the results directly. Write $t = t_N/(t_D + t'_D)$ and we have

$$t_N = 2(\phi + \phi')\cos(\theta)e^{-ik_0 L} \quad t_D = e^{ikL}(\phi - e^{-i\theta})(e^{i\theta} - \phi') \quad t'_D$$
$$= e^{-ikL}(\phi + e^{i\theta})(\phi' + e^{-i\theta}) \quad (6)$$

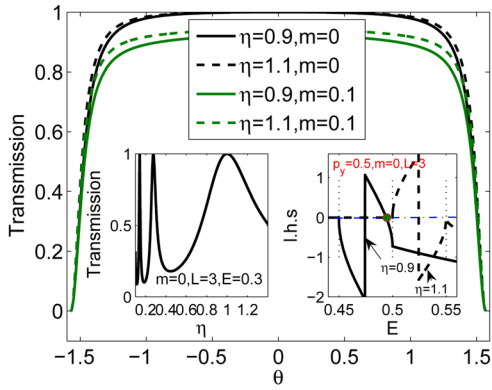from which we find (in the case of vanishing mass) for real k

FIG. 2. (Color online) T vs θ at $E = 0.3$ and $L = 3$. The left inset shows T as a function of $\eta = v/v_0$. The right one locates the localized modes [refer to Eq. (10) for details], which are marked with green spots.

$$T = \frac{\cos^2\varphi\cos^2\theta}{\cos^2\varphi\cos^2\theta + 4\sin^2(kL)\sin^2\left(\dfrac{\theta-\varphi}{2}\right)\cos^2\left(\dfrac{\theta+\varphi}{2}\right)} \tag{7}$$

whereas for imaginary k

$$T = \frac{|t_N|^2}{|t_D + t_D'|^2}; \quad |t_N|^2 = 4\sinh^2\psi\cos^2\theta$$

$$|t_D + t_D'|^2 = e^{-2\kappa L}\{(\sin\theta + \sinh\psi)^2 + 2\cos^2\theta\}$$
$$+ e^{2\kappa L}(\cosh^2\psi - \sin^2\theta)^2$$
$$- 2\left\{1 + \sin\theta[\sinh\psi - \cosh\psi] + \frac{\sinh(2\psi)\cos(2\theta)}{2}\right\} \tag{8}$$

where we have introduced $(k_y, \kappa) = E/\hbar v(\cosh\psi, \sinh\psi)$. From Eq. (7), we see that $T = 1$ for $\theta = 0$ (and $m = 0$).

Interestingly, there is a scaling invariance associated with t. To see this, we introduce a system of units: [Length] $= (\sqrt{3}a_0/2)R$, [Energy] $= \gamma_0/R$, [Momentum] $= \hbar/$[Length], [Velocity] $=$ [Length][Energy]$/\hbar$ and [wavevector] $= 1/$[Length], where a_0 is the in-plane C−C bond length, γ_0 represents the nearest neighbor electron hopping energy, and R is just the scaling parameter. Obviously, t (and the Fermi velocity) does not depend on R. We shall adopt this unit system in the numerical results given below.

In Fig. 2, we display T as a function of the incidence angle θ at fixed L and E. The parameters (m, η) are chosen to
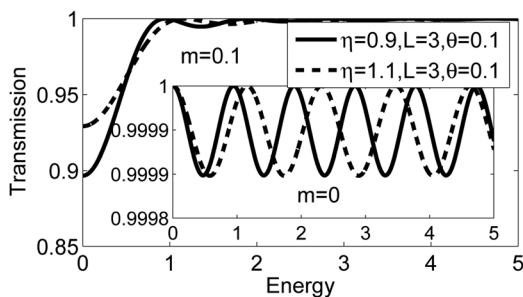

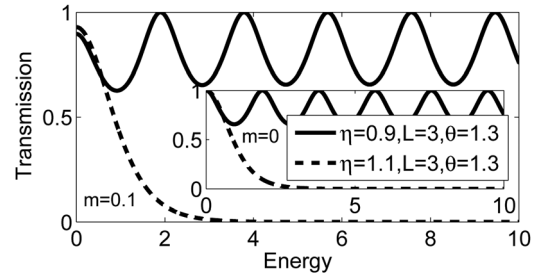FIG. 3. Transmission vs energy at $m = 0.1$, for small θ. Inset: the same but $m = 0$.

FIG. 4. Transmission vs energy at $m = 0.1$, for big θ. Inset: the same but $m = 0$.

cover four possibilities with m either small or vanishing and η either a little larger or smaller than unity, which are experimentally accessible. As seen in this figure, there exists such an angle $\theta_c \approx 1.1$ that for $0 < \theta < \theta_c$, T is around unity (Actually, $T_{\theta=0} = 1$) almost regardless of θ while for $\theta > \theta_c$ a sharp drop occurs. This behavior is also manifested in the E and L dependence of T, as exhibited in Figs. 3–6. In Fig. 3, we plot T against E for $\theta < \theta_c$. As seen in this figure, the two curves corresponding to $\eta > 1$ and $\eta < 1$, respectively, are similar, be the mass vanishing or not. For small mass, T resembles what happens in the usual nonrelativistic scattering in the presence of a potential barrier while for $m = 0$, T oscillates as simple harmonics. However, as shown in Fig. 4, the situation with $\theta > \theta_c$ is dramatically different. For $\eta < 1$, sheer oscillation is seen. But for $\eta > 1$, within the energy range displayed, T decays to zero steeply as energy increases. The T as a function of L follows similar trends, as seen in Figs. 5 and 6. Clearly observed in the inset of Fig. 6, for $\eta > 1$, high energy incident electrons can be nearly perfectly reflected by choosing proper L and $\theta > \theta_c$.

Such phenomena obviously stems from TIR. Actually, the angle θ_c can be evaluated via Eq. (5), which yields $\theta_c \approx 1.1$, consistent with what was numerically perceived above. Moreover, they were seen to occur only for $\eta > 1$, as expected from TIR. The phenomena may be utilized to filter high energy electrons or switch an electrical circuit through, e.g., simply varying the gate voltage. Suppose an SLG is deposited on top of a prepatterned substrate and a gate is placed on the SLG. The substrate may be laid down in such a fashion that the channel lies along a direction that makes an angle with the x-direction. When electrons flow along the device, this angle is simply the incidence angle θ. One can set it to be larger than θ_c. At low temperatures, the device conductance should be simply proportional to $T_\theta(E = \mu)$,[22] where μ denotes the chemical potential. The μ and hence the conductance can be tuned by changing the gate voltage.
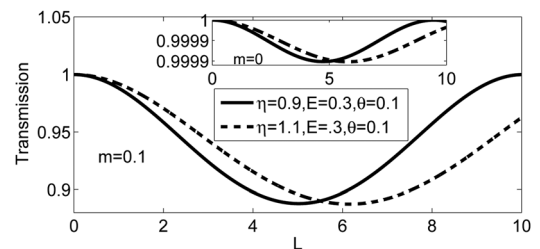

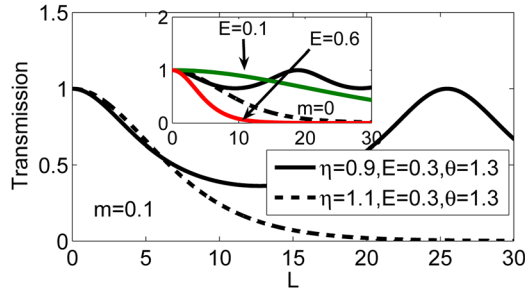FIG. 5. Transmission vs L at $m = 0.1$, for small θ. Inset: the same but $m = 0$.

FIG. 6. (Color online) Transmission vs L at $m = 0.1$, for big θ. Inset: the same but $m = 0$.

III. LOCALIZED STATES

We now examine the existence of localized states. Consider the interface states first. These are supposed to be localized about a boundary. Take the boundary at $x = 0$ for instance. The wavefunction then reads

$$
\begin{aligned}
\Phi(x < 0) &= A e^{\kappa_0 x} \begin{pmatrix} i \dfrac{\hbar v_0(\kappa_0 + k_y)}{E} \\ 1 \end{pmatrix} \\
\Phi(x > 0) &= B e^{-\kappa x} \begin{pmatrix} i \dfrac{\hbar v(\kappa - k_y)}{E - m} \\ 1 \end{pmatrix}
\end{aligned} \tag{9}
$$

where the κ_0 and κ play role in $E^2 = \hbar^2 v_0^2(k_y^2 - \kappa_0^2)$ and $E^2 = \hbar^2 v^2(k_y^2 - \kappa^2) + m^2$, respectively. Now we match the Φ at $x = 0$ and then obtain the following secular equation determining the value of E,

$$
\frac{k_y + \sqrt{k_y^2 - \dfrac{E^2}{\hbar^2 v_0^2}}}{\sqrt{k_y^2 - \dfrac{E^2 - m^2}{\hbar^2 v^2}} - k_y} = \frac{v}{v_0} \cdot \frac{E}{E - m} \tag{10}
$$

whose solutions can exist only in $(-m, 0]$. Actually, it has a single solution at $E = 0$ for $k_y = 0$ and $m \neq 0$. No solution exists for $m = 0$ or $k_y \neq 0$.

Another type of localized states oscillate in the channel but decay in both electrodes. Their wave functions are then formed as

$$
\begin{aligned}
\Phi_L &= A e^{\kappa_0 x} \begin{pmatrix} -i \dfrac{\hbar v_0(\kappa_0 + k_y)}{E} \\ 1 \end{pmatrix} \\
\Phi_R &= A' e^{-\kappa_0 x} \begin{pmatrix} i \dfrac{\hbar v_0(\kappa_0 - k_y)}{E} \\ 1 \end{pmatrix} \\
\Phi_C &= B e^{ikx} \begin{pmatrix} \dfrac{\hbar v |\vec{k}| e^{-i\varphi}}{E - m} \\ 1 \end{pmatrix} + B' e^{-ikx} \begin{pmatrix} \dfrac{\hbar v |\vec{k}| e^{i\varphi}}{m - E} \\ 1 \end{pmatrix}
\end{aligned} \tag{11}
$$

Matching Φ at both $x = 0$ and $x = L$, we find a similar secular equation as

$$
\begin{aligned}
&(\kappa_0 - k_y)\cos(kL + \varphi) + (\kappa_0 + k_y)\cos(kL - \varphi) \\
&= \frac{2E^2 \sin(kL)}{\hbar^2 v v_0 |\vec{k}|}
\end{aligned} \tag{12}
$$

which, in the case where $m = 0$, reduces to

$$
\arctan\left(\frac{\sqrt{E^2 - \hbar^2 v^2 k_y^2} \cdot \sqrt{\hbar^2 v_0^2 k_y^2 - E^2}}{E^2 - \hbar^2 v v_0 k_y^2} \right) = kL \tag{13}
$$

whose solutions must lie in $[\eta^2, 1]v_0^2 k_y^2$, implying the requirement of $\eta < 1$. Numerical examples have been demonstrated in the inset of Fig. 1, where one solution is seen for $\eta = 0.9$ while none solution for $\eta = 1.1$, as expected. As an application, this kind of state may motivate one to make an electron box, as often realized with quantum dots.

SUMMARY AND ACKNOWLEDGEMENT

In summary, we have studied the electronic states of a hybrid graphene structure. Dirac-type Hamiltonian has been employed to describe the electronic degrees of freedom. The Dirac cones are supposed of different slopes and possibly somewhat warped. The scattering states are investigated and the transmission probability is obtained. Discussions have been performed in parallel with optics. Both Snell-type law and TIR have been derived for graphene electrons. Such TIR has been found to have remarkable impacts on electronic transmission. Especially, below the TIR critical angle θ_c, the transmission is shown close to 100%. Whereas above it, high energy electrons are almost perfectly impeded, leaving low energy electrons passing through the channel very well. This property has been proposed to make an electron filter or electrical switch. We have also examined two kinds of localized states in the structure. Interface states were found to exist only if $m \neq 0$ and $k_y = 0$, while states confined to the channel have been found for $\eta < 1$. The latter states may be utilized to create nano graphene dots. Two routes have been proposed to realize such structure: one is to lay down an SLG on prepatterned substrate, while another by manipulation of twisted BLG.

[1] K. S. Novoselov, A. K. Geim, S. V. Morozov, D. Jiang, Y. Zhang, S. V. Dubonos, I. V. Grigorieva, and A. A. Firsov, Science **306**, 666 (2004); K. S. Novoselov, D. Jiang, F. Schedin, T. J. Booth, V. V. Khotkevich, S. V. Morozov, and A. K. Geim, PNAS USA **102**, 10451 (2005).

[2] A. K. Geim and K. S. Novoselov, Nature Mater. **6**, 183 (2007).

[3] N. M. R. Peres, Rev. Mod. Phys. **82**, 2673 (2010).

[4] P. R. Wallace, Phys. Rev. **71**, 622 (1947).

[5] Y. Zhang, J. W. Tan, H. L. Stormer, and P. Kim, Nature **438**, 201 (2005).

[6] A. H. Castro Neto, F. Guinea, N. M. R. Peres, K. S. Novoselov, and A. K. Geim, Rev. Mod. Phys. **81**, 109 (2009).

[7] C.-H. Park, F. Giustino, M. L. Cohen, and S. G. Louie, Nano Lett. **8**, 4229 (2008).

[8] C.-H. Park, F. Giustino, C. D. Spataru, M. L. Cohen, and S. G. Louie, Phys. Rev. Lett. **102**, 076803 (2009).

[9] J. Wang, H. A. Fertig, G. Murthy, and L. Brey, Phys. Rev. B **83**, 035404 (2011).

[10] L. Yang, M. L. Cohen, and S. G. Louie, Nano Lett. **7**, 3112 (2007).

[11] L. Yang, J. DEslippe, C.-H. Park, M. L. Cohen, and S. G. Louie, Phys. Rev. Lett. **103**, 186802 (2009).

[12] G. Borghi, M. Polini, R. Asgari, and A. H. MacDonald, Solid State Commun. **149**, 1117 (2009); C. Attaccalite and A. Rubio, Phys. Status Solidi B **246**, 2523 (2009).

[13]M. Calandra and F. Mauri, Phys. Rev. B **76**, 205411 (2007).

[14]P. E. Trevisanutto, C. Giorgetti, L. Reining, M. Ladisa, and V. Olevano, Phys. Rev. Lett. **101**, 226405 (2008).

[15]C.-H. Park, F. Giustino, C. D. Spataru, M. L. Cohen, and S. G. Louie, Nano Lett. **9**, 4234 (2009).

[16]C.-H. Park, L. Yang, Y.-W. Son, M. L. Cohen, and S. G. Louie, Nat. Phys. **4**, 213 (2008).

[17]C.-H. Park, L. Yang, Y.-W. Son, M. L. Cohen, and S. G. Louie, Phys. Rev. Lett. **101**,126804 (2008).

[18]A. Luican, G. Li, A. Reina, J. Kong, R. R. Nair, K. S. Novoselov, A. K. Geim, and E. Y. Andrei, Phys. Rev. Lett. **106**,126802 (2011).

[19]E. Suárez Morell, J. D. Correa, P. Vargas, M. Pacheco, and Z. Barticevic, Phys. Rev. B **82**, R121407 (2010); S. Shallcross, S. Sharma, and O. A. Pankratov, Phys. Rev. Lett. **101**, 056803 (2008); E. J. Mele, Phys. Rev. B **81**, R161405 (2010).

[20]S. Shallcross, S. Sharma, E. Kandelaki, and O. A. Pankratov, Phys. Rev. B **81**, 1 (2010).

[21]A. Reina, X. Jia, J. Ho, D. Nezich, H. Son, V. Bulovic, M. S. Dresselhaus, and J. Kon, Nano Lett. **9**, 3087 (2009).

[22]J. W. González, H. Santos, M. Pacheco, L. Chico, and L. Brey, Phys. Rev. B **81**, 195406 (2010); S. Datta, Electronic Transport in Mesoscopic Systems (Cambridge University Press, Cambridge, 1995).